Utilization of a cell-penetrating peptide-adaptor for delivery of human papillomavirus protein E2 into cervical cancer cells to arrest cell growth and promote cell death

Julia C. LeCher[1], Hope L. Didier[2], Robert L. Dickson[2], Lauren R. Slaughter[2], Juana C. Bejarano[2], Steven Ho[2], Scott J. Nowak[2], Carol A. Chrestensen[3] and Jonathan L. McMurry[2*]

[1]Center for ViroScience and Cure, Laboratory of Biochemical Pharmacology, Department of Pediatrics, Emory University School of Medicine, Atlanta, GA 30322, USA

[2]Department of Molecular & Cellular Biology, Kennesaw State University, 370 Paulding Ave NW, MD 1201, Kennesaw, GA 30144, USA

[3]Department of Chemistry & Biochemistry, Kennesaw State University, 370 Paulding Ave NW, MD 1201, Kennesaw, GA 30144, USA

JCL: jlecher@emory.edu; HLD: hdidier@wakehealth.edu; RLD: dickson.305@osu.edu; LRS: lauren.slaughter@midwestern.edu; JCB: j.camilabejarano@gmail.com; SH: stevenho2015@gmail.com; SJN: snowak@kennesaw.edu; CAC: cchreste@kennesaw.edu; JLM: jmcmurr1@kennesaw.edu

*Corresponding author, 470-578-3238 (telephone), 470-578-9136 (fax), jmcmurr1@kennesaw.edu

Conflicts of Interest: The authors declare no conflict of interest.

Data Availability Statement: The data that support the findings of this study are available from the corresponding author upon reasonable request.

Abstract

Background: Human papillomavirus (HPV) is the causative agent of nearly all forms of cervical cancer, which can arise upon viral integration into the host genome and concurrent loss of viral regulatory gene E2. Gene-based delivery approaches show that E2 reintroduction reduces proliferative capacity and promotes apoptosis in vitro. This work explored if our calcium-dependent protein-based delivery system, TAT-CaM could deliver functional E2 protein directly into cervical cancer cells to limit proliferative capacity and induce cell death.

Methods: TAT-CaM and the HPV16 E2 protein containing a CaM-binding sequence (CBS-E2) were expressed and purified from *E. coli*. Calcium-dependent binding kinetics were verified by Biolayer Interferometry. Equimolar TaT-CaM:CBS-E2 constructs were delivered into the $HPV16^{+}$ SiHa cell line and uptake verified by confocal microscopy. Proliferative capacity was measured by MTS assay and cell death was measured by release of lactate dehydrogenase. As a control for specificity to HPV^{+} cells, human microvascular cells (HMECs) were used.

Results: TAT-CaM bound CBS-E2 with high affinity in the presence of calcium and rapidly disassociated in its absence. After introduction by TAT-CaM, E2 was detected in cellular interiors by orthogonal projects taken at the depth of the nucleus. In dividing cells, E2 relocalized to regions associated with the mitotic spindle. Cells receiving a single daily dose of CBS-E2 for 4 days showed a significant reduction in metabolic activity at low doses and cell death at high doses compared to controls. This phenotype was retained for 7 days with no further treatments. When subcultured at day 12, treated cells regained their proliferative capacity.

Conclusions: Using the TAT-CaM platform, bioactive E2 protein was delivered into living cervical cancer cells, inducing senescence and cell death in a time- and dose-dependent manner. These results suggest that this nucleic acid and virus-free delivery method could be harnessed to develop novel, effective protein therapeutics.

Keywords: cell-penetrating peptides, cervical cancer, HPV-16, E2, E6, E7

1. Introduction

Human papillomavirus is a sexually transmitted virus and the causative agent of multiple forms of cancer including cervical, vaginal, oropharyngeal, anal, penile and vulvar and is the second leading cause of cancer-related death in women worldwide (1). Globally, this is partly attributed to a lack of access to preventive care and early detection, particularly in middle and low-income nations. Further, metastatic cervical cancer remains difficult to treat and retains high 5-year recurrence rates. Recent years have seen a surge in clinical trials aimed at developing new immunotherapies to increase survival rates and reduce effective doses of traditional, harsher treatments, but only one drug, Avastin, has been approved in the U.S. HPV-mediated cervical cancer thus remains a significant global burden and new treatment approaches are wanting.

A key event in many HPV-mediated cancers is viral integration into the human genome. During primary infection, HPV infects undifferentiated cells of the cervical basal epithelium. New virions exit from terminally differentiated cells in the outer layer of the cervical epithelium. The virus thus requires proliferation and subsequent differentiation of host endodermal cells up the cervical epithelial wall for egress of new virions (2). To insure this occurs, HPV encodes two proteins, E6 and E7, that inhibit apoptotic pathways and promote cellular proliferation, respectively (3, 4). Another viral protein, E2, regulates E6 and E7 at the level of transcription and via direct protein binding (5-7). In over 80% of HPV carcinomas the E2 open reading frame (ORF) is the primary site of viral integration. Integration often results in the loss of E2 but retention of the E6 and E7 ORFs (8-12). This promotes unregulated overproduction of E6 and E7 which, in turn, can lead to cellular changes promoting carcinogenesis. Loss of E2 is thought to be a critical event in the onset of many integrated HPV cancers.

Given its regulatory role of inhibiting E6 and E7, in 1993 Hwang et al. hypothesized that replenishment of E2 in cervical cancer cells could halt their proliferation and reverse their metastatic potential (13). They, and others, demonstrated that reintroduction of E2 into cervical cancer cells could induce cell senescence (13-15). Later work showed that E2 overexpression after gene delivery promotes apoptosis (16, 17). However promising, this approach has not become a viable treatment option for cancer patients likely owing to the need for gene transfection, a

technical challenge in and of itself (18). In 2004, Roeder et al. described the use of the HSV cell-penetrating peptide (CPP), VP22, to deliver VP22:E2 fusion proteins into cervical cancer cell lines for the induction of apoptosis (19). In this, and later studies, VP22:E2 fusion proteins were made from plasmids introduced into cells and, once translated, these fusion proteins were secreted from transformed cells and readily entered other neighboring cells to promote cell death (19, 20). In this study we developed a more direct approach for E2 protein delivery using a CPP TAT-CaM adaptor.

CPPs are short peptides that can readily cross cell membranes and can confer that ability on biomolecules to which they are attached. CPP attachment is most commonly via covalent bond or nonspecific hydrophobic interaction. However, these CPP-cargos often become trapped in endosomes upon cellular entry and, as a result, become targeted for degradation, resulting in cargo destruction rather than delivery to the cytoplasm or subcellular destination (21). Our adaptor, "TAT-CaM", consists of well-known CPP, TAT, fused to a human calmodulin (CaM) (22, 23). Cargo proteins are engineered to contain a calmodulin binding sequence (CBS). Given that the extracellular environment contains relatively high levels of calcium, complexes remain tightly associated upon entry into the cell. However, during endosomal trafficking, calcium efflux results in cargo dissociation from TAT-CaM and subsequent release to the cytoplasm of living mammalian cells. Delivery is rapid, tunable and efficient and a wide variety of cargos can be delivered into living cells (22-24)

Using the TAT-CaM adaptor system, the hypothesis that bioactive CBS-E2 protein delivered directly into cervical cancer cells would inhibit cellular proliferation and/or cell death was tested. Following delivery, E2 showed distinct cell-cycle dependent subcellular localization patterns and was found in both the cytoplasm and the nucleus. In mitotic cells, E2 relocalized to regions of the cell associated with the mitotic spindle, a known biological activity (25). As expected, E2 prohibited cellular proliferation and promoted cell death in a time and dose-dependent manner supporting a model wherein E2 reduces cellular proliferation at low cell-to-peptide ratios and promotes cell death at high cell-to-peptide ratios. These data also further validate the TAT-CaM adaptor and provide a new framework for delivery of E2 protein into living cells.

2. Materials & Methods

112 *2.1 Generation and purification of CBS-E2 and TAT-CaM constructs*

113 An *E. coli*-optimized synthetic gene encoding the E2 ORF from HPV-16 was cloned into pCAL-
114 N-FLAG (Agilent Technologies, CA, USA), which contains a vector-encoded N-terminal
115 calmodulin bind site (CBS). CBS-E2 and TAT-CaM were expressed and purified as previously
116 described with slight modifications (22). Briefly, CBS-E2 was expressed in ArcticExpress (DE3)
117 *E. coli* cells (Agilent Technologies, USA) and purified by fast protein liquid chromatography using
118 Calmodulin-Sepharose (GE Healthcare, USA). TAT-CaM was expressed in BL21(DE3)pLysS *E.*
119 *coli* cells (Agilent Technologies, CA, USA) and purified to near-homogeneity by metal-affinity
120 chromatography using TALON resin (Takara Bio, USA). After purification, protein constructs
121 were dialyzed into calcium-containing binding buffer (10 mM HEPES, 150 mM NaCl, 2 mM
122 $CaCl_2$, 10% glycerol pH 7.4), sterilized via syringe-driven filtration through a 0.22 µm filter, flash
123 frozen in liquid nitrogen and stored at -80°C until use. Samples were collected at each stage of the
124 purification process in 2% SDS buffer and subjected to gel electrophoresis as previously described
125 (26). Elutions were further subjected to western blot analysis as previously described using an HPV
126 16 E2 monoclonal primary antibody TVG 621 (ThermoFisher, USA) and goat anti-mouse HRP
127 conjugated secondary (ThermoFisher, USA) (26).

128 *2.2 Biolayer Interferometry*

129 Biolayer interferometry (BLI) experiments were performed on a FortéBio Octet QK (Menlo Park,
130 CA, USA) as previously described (22). Biotinylated TAT-CaM was loaded onto streptavidin (SA)
131 sensors for 300 s in binding buffer followed by a 180 s baseline measurement. TAT-CaM ligand
132 was then exposed to analyte CBS-E2 and association was measured for 300 s. Two different
133 dissociation phases followed, each 300 s in length. Ligand:analyte pairs were first exposed to
134 binding buffer and were then challenged in binding buffer containing 10 mM EDTA. Baseline drift
135 as measured by a parallel run in which a ligand-loaded sensor was exposed to buffer only was
136 subtracted from each experimental run. Fast-on, slow-off binding was fit to a global 1:1
137 association-then-dissociation model and EDTA-induced rapid dissociation was separately fit to a
138 one-phase exponential decay model using GraphPad Prism 5.02 software. Nonspecific binding, as
139 measured by a run of a sensor without ligand exposed to the highest concentration of CBS-E2,
140 evinced negligible binding and was ignored in analysis.

141 *2.3 Cell culture*

142 The HPV-16+ cell line SiHa (ATCC© HTB-35) and the Human Microvascular Endothelial Cell
143 line (HMEC; CRL-3243) were purchased from ATCC (Manassas, VA, USA). SiHas were cultured
144 in glucose-free complete Dulbecco's Minimal Eagle Media (DMEM; Gibco™ ThermoFisher,
145 USA) with 10% fetal bovine serum (FBS; Atlas Biologicals) and 1 mM L-glutamine (Gibco™
146 ThermoFisher, USA). HMECs were cultured in MCDB131 media containing 10% FBS, 10 mM
147 L-Glutamine, 10 ng/mL human recombinant epidermal growth factor (EGF; Gibco™
148 ThermoFisher, USA), and 1 ug/mL hydrocortisone (Gibco™ ThermoFisher, USA). Both cell lines
149 were maintained in a humidified incubator at 37°C with 5% CO_2 injection.

150 *2.4 Confocal microscopy*

151 All confocal experiments were performed on an inverted Zeiss LSM700 confocal microscope
152 equipped with a humidified incubator at 37°C with 5% CO_2 injection as previously described (22).
153 In short, SiHa cells were plated at ~50% confluency in 4-well Nunc Lab-Tek chambered
154 coverglass wells (ThermoFisher, USA) 16 hours prior to cell penetration assays. CBS-E2 cargos
155 were labeled with DyLight 550 (ThermoFisher, USA) or left unlabeled (experimental control) then
156 incubated with or without (experimental control) TAT-CaM in equimolar amounts (1 µM) in
157 binding buffer. Complexes were then added to glucose-free DMEM and introduced to cells.
158 Uptake was performed in a humidified incubator at 37°C with 5% CO_2 injection for 1 hr with
159 periodic rocking (every 15 mins) to ensure even distribution. After 1 hr, media were removed and
160 cells washed 5x with calcium-containing phosphate buffered saline (PBS; 1mM $CaCl_2$). Next, cells
161 were counterstained with 2 µM CellTracker Green CMFDA dye (ThermoFisher, USA) and 3 µM
162 NucBlue (ThermoFisher, USA) per manufacturer's protocols to stain the cytoplasmic and nuclear
163 compartments of the cells respectively. After staining, cells were washed 3x with calcium-
164 containing PBS and full cell culture media was added to each well. For live-cell uptake with
165 downstream immunofluorescence, after treatment cells were counterstained with NucBlue only
166 then fixed in ice-cold 100% methanol for 3 minutes. Fixed cells were blocked (PBS + 2% FBS),
167 incubated overnight with primary antibody beta-tubulin in PBS + 0.1% Triton-X-100, washed 3x
168 with PBS, incubated for 1 hr with GFP-conjugated secondary antibody, washed 3x with PBS,
169 mounted and visualized. Cells were imaged using a 40x EC Plan-Neofluar objective with a NA

value of 1.3. Image analysis was performed on Zen Blue software (Carl Zeiss Microscopy, Germany) as previously described (22).

2.5 Analysis of cellular proliferation and cell death

Cellular proliferation was assayed by ability to metabolize 3-(4,5-dimethylthiazol-2-yl)-5-(3-carboxymethoxyphenyl)-2-(4-sulfophenyl)-2H-tetrazolium (MTS; CellTiter 96® AQ_{ueous} One Solution Cell Proliferation Assay by Promega, USA). In the same population of cells, cell death was assayed by release of lactate dehydrogenase (LDH) into cell culture media (CytoTox 96® Non-Radioactive Cytotoxicity Assay by Promega, USA). Cells were seeded into 96-well plates at either 2.5 $x10^3$ or 2.5 $x10^4$ in 100 µL of phenol-red free cell culture media and allowed to adhere to the plate overnight (Day 0). The next day (Day 1) cells were treated with increasing amounts of CBS-E2 with equimolar TAT-CaM in binding buffer, TAT-CaM only (vehicle control), buffer (experimental control) or simply left untreated. After 1 hr, treatments were removed and 100 µL of cell culture medium was added to each well. Treatments were repeated at 24 and 48 hrs. Every 24 hrs, 50 µL of medium was transferred to another 96 well plate and assayed for LDH per manufacturer's protocol. At 72 hrs (Day 4), MTS reagent was added directly to cells and cells were assayed for MTS metabolism per manufacturer's protocol. A BioTek multimode plate reader (BioTek Instruments, VT, USA) was used to measure OD_{490}. Absorbance due to metabolic or LDH activity was calculated by subtracting background (cells with no reagent) from total. Percent metabolic activity (MTS assay) was calculated using the following equation: $(OD_{treated}/OD_{untreated})$ x 100. Percent cell death (LDH assay) calculated using the following equation: $(OD_{untreated}/OD_{treated})$ x 100.

2.6 Statistical Analysis

All analysis was performed on GraphPad Prism 8.0 software. Treated groups were compared to the untreated group using one-way or two-way ANOVA with either Dunnet's or Tukey's correction for multiple comparisons as indicated in figure legends. Deviation was calculated using standard error of the mean.

3. Results

198 *3.1 CBS-E2 binds TAT-CaM with expected kinetics.*

199 Our previous work validated that TAT-CaM binds model CBS-cargo proteins rapidly and
200 stably in the presence of calcium and dissociates almost instantaneously and completely when
201 calcium is removed (22, 23). In this study we expressed and purified an E2 construct from HPV-
202 16 that contained an N'terminal CBS tag (Supplemental Figure 1). Calcium-dependent binding
203 kinetics of TAT-CaM with CBS-E2 were analyzed via biolayer interferometry (**Fig. 1**). Fits to a
204 single-state association-then-dissociation model (**Fig. 1A**) yielded a calcium-replete K_D of 36 nM
205 with k_{on} = 4.6 x 10^4 $M^{-1}s^{-1}$ and k_{off} = 1.6 x 10^{-3} s^{-1}. In the presence of the chelating agent EDTA,
206 dissociation was very rapid (**Fig. 1B**). $k_{off(EDTA)}$ was 5.3 x 10^{-2} s^{-1}. These data validate the utility
207 the TAT-CaM approach for delivery of E2.

208 *3.2 Live cell uptake and cellular redistribution of CBS-E2 post TAT-CaM-mediated delivery*

209 TAT-CaM was used to deliver free bioactive E2 protein into the human HPV-16+ cervical
210 cancer cell line SiHa. Given significant artifacts resulting from fixation that have confounded
211 results in the past, live cell imaging in asynchronous populations of human cervical cancer cells
212 was performed. *Z*-stacks were acquired via confocal microscopy and analyzed for intracellular
213 delivery of fluorescently labeled CBS-E2 in the presence of TAT-CaM (**Fig. 2B**). To verify that
214 TAT-CaM mediated entry, parallel control experiments without TAT-CaM were performed (**Fig.**
215 **2A**). In the presence of TAT-CaM, CBS-E2 was readily delivered into cells (**Fig. 2B**), while in the
216 absence of TAT-CaM negligible signal was observed (**Fig. 2A**). One biological property of HPV
217 E2 proteins is the ability to localize to the mitotic spindle during cellular division (25, 27). Circular
218 clusters of E2 formed on DNA were observed at the onset of mitosis (white arrows; **Fig. 2C,D**),
219 suggestive of localization to aster microtubules as previously described (25, 27). In cells
220 undergoing anaphase and telophase (as determined by visual observation of nuclear staining
221 patterns), CBS-E2 clustered on the midplane (white arrows; **Fig. 2E, F**). Further, live cell uptake
222 coupled to downstream immunofluorescence showed co-localization of E2 with beta-tubulin
223 around the nucleus in cells visually undergoing mitosis (**Sup. Fig. 2**) These data demonstrate that
224 CBS-E2 was delivered in bioactive form.

225 *3.3 E2 inhibits cell progression and induces cell death in cervical cancer cells.*

Previous studies showed that transfection of cervical cancer cells with E2 is sufficient for induction of senescence or apoptosis within 3 days (13-16). An experimental limitation to the use of gene delivery is lack of control of dose, i.e. how much protein is made in the cell after transfection. To test if CBS-E2 could induce senescence and/or cell death by direct protein delivery, experiments were designed to determine how much protein would be required over 3 days. As a starting point, 2.5 x 10^4 cells were treated daily for 3 days with 1 or 4 μM doses of CBS-E2 and equimolar TAT-CaM. At 1 μM there was no significant effect on cells post E2 delivery, while at 4 μM, there was a 28% reduction in metabolic activity on day 4 (**Fig. 3A**). Total cell counts were also performed at day 4. Untreated and TAT-CaM only treated groups showed similar growth rates while cells treated with 4 μM E2 failed to proliferate (**Fig. 3B**). Microscopic analysis of cells on day 4 further corroborated these findings (**Fig 3. C-E**). Untreated and TAT-CaM treated cells exhibited normal morphology while E2 treated cells overwhelming became flattened out, with a loss in typical spindle-like morphology, and exhibited intracellular stress granule-like formations (**Fig. 3E**). Collectively, these data support that 3 doses of CBS-E2 protein over 3 days is sufficient to significantly reduce cellular proliferation within this population of cells.

Persistence of this phenotype was assayed by retaining cells in culture for an additional week with regular media changes. Over 12 days, with no additional E2 treatments, cells from the 4 μM CBS-E2 treated group showed a significant reduction in metabolic activity (**Fig. 3A**) and failed to proliferate while untreated cells and those dosed with TAT-CaM only retained normal doubling times (**Fig. 3B**). Microscopic analysis supported these findings (**Fig. 3 F-H**). In untreated and TAT-CaM-treated groups, cells became over-confluent and crowded the wells (Fig 3F, G). CBS-E2-treated cells showed no increase in cell number (**Fig. B**), however, some cells within the population regained normal spindle-like morphology (**Fig. 3H**). We hypothesized that these cells might represent a subpopulation of harder to treat persister cells. To test for this, cells were collected and re-seeded at equal density. After 7 days in culture, cells were collected and counted (**Fig 3I**). E2-treated cells regained normal growth kinetics (**Fig. 3I**) and normal morphology (**Fig 3B)** indistinguishable from untreated or TAT-CaM treated cells. These data suggest that at the cell-to-peptide ratios employed only a sub-population of cells underwent senescence while others were seemingly unaffected or more resistant to E2's effects.

3.4 Dose-dependent effect of E2 on cellular proliferation and cell death.

To test the effect of cell-to-peptide ratios a dose-response assay was performed using the same protocol with the exception that the starting cell number was lowered 10-fold. While 0.1 μM doses had little effect, cells showed a dramatic reduction in metabolic activity at only 1 μM (75% loss; **Fig. 4A**). Similar observations were made with 10 μM doses, suggesting that at doses >1 μM there is a 'plateau effect,' in that higher doses had no discernible increased effect (**Fig. 4A**). Within the same population of cell, cell death was tested each day by measuring total LDH levels in the media. Results showed significantly high levels of LDH in all E2 treatment groups (Fig. 4B). The much smaller level of LDH activity in controls was attributed to retention of normal growth rates leading to overconfluency. Next, E2's ability to induce cell death in a non-cervical cancer human microvascular endothelial cell line (HMEC) was tested. The same LDH leakage assay was performed as above using the highest dose group of TAT:CaM & CBS-E2 (10 μM) in both SiHa and HMEC cell lines. SiHas showed significantly higher levels of cell death when compared with all other treatment groups while there was no discernible effect on HMECs following E2 delivery (**Fig. 5A**). Microscopic analysis of cells on day 3 qualitatively corroborated these results (**Fig. 5 B-D**). Collectively, these data support the hypothesis that direct delivery of E2 protein into living cervical cancer can inhibit cellular proliferation or induce cell death and, further, suggest that these differential outcomes may be a function of dose. Further, that E2 did not induce cell death in the HMEC cell line support a specificity for HPV^+ cells.

4. Discussion

In this study we describe our use of the efficient, high-affinity reversible TAT:CaM adaptor system for CPP-mediated delivery of E2 to cell interiors that exploits natural extra- and intracellular levels of calcium. CBS-E2 cargos were readily delivered into $HPV16^+$ cells and showed evidence of sub-cellular relocalization during cell division. Over time, CBS-E2 reduced cellular proliferation rates and metabolic activity as well as induced cell death.

CBS-E2 showed expected high affinity, calcium-dependent binding kinetics with TAT-CaM (**Fig. 1**). While K_D was slightly lower and k_{off} in EDTA slower than observed for CaM binding to endothelial nitric oxide synthase (NOS3), a native CBS-containing protein (28), they were in well within the range of constants previously determined for TAT-CaM other cargo proteins (22, 23). Plateaus observed in the EDTA dissociation phase are confounding in that

complete dissociation ought to result in a plateau of 0 nm shift given that non-specific binding of analyte to the sensor was near zero. However, similar plateaus have been previously observed with CaM and analytes in BLI and were attributed to partial denaturation of the proteins, perhaps a result of tethering to the sensor (29). Another contributor is uncertainty of the value of Y_0 (Y at the beginning of dissociation) as dissociation is very rapid and the instrument takes a reading only every 1.6 s. For very fast processes, there is also often a discontinuity between the end of one phase, in this case dissociation in Ca^{2+}, and the next, dissociation in EDTA. Indeed, the residuals (**Fig. 1B**) indicate the poorest fit at the outset of dissociation, though they remain within the range of normal for the BLI instrument. Regardless of the idiosyncratic uncertainties inherent in the measurements, the kinetics of the interaction were as expected and suitable for delivery of CBS-E2 into cells.

TAT-CaM readily delivered CBS-E2 constructs into the HPV-16+ cervical cancer cell line SiHa (Fig. 2). Over the course of the cell penetration assays, a distinctive and repeatable pattern of intracellular localization in mitotic cells to regions associated with mitotic spindle fibers was observed (**Fig. 2C-F)** as well as co-localization with beta-tubulin **(Sup. Fig. 2**). While both low-risk (LR) and high-risk (HR) E2 proteins can associate with the spindle, the manner of association and resultant distribution pattern of LR vs HR E2s during mitosis differs (25, 27). High-risk HPV E2 proteins initially cluster at the asters at the onset of mitosis (25). As the cell progresses through mitosis, E2 relocates to the midplane where it associates with the Anaphase Promoting Complex (APC/C) (25, 27, 28, 30) and remains at the midbody through cytokinesis. In concordance with these results, mitotic cells in cell-penetration experiments showed a distinctive pattern of CBS-E2 redistribution as previously noted for HR E2.

In this work, CBS-E2 readily inhibited cellular proliferation (**Fig. 3 A,B)** and promoted cell death in HPV^+ cells (**Fig. 4)** similar to that as previously reported in E2 reintroduction studies **(**13-17**,** 19**,** 20**).** TAT-CaM-only treated cells exhibited upwards of 18% cytotoxicity in SiHa cells when starting cell counts were sub-confluent (10^3; **Fig. 4B**), however no toxicity was noted at this dosage with 10-fold higher starting cell counts (10^4; **Fig. 3A**). This is a documented phenomenon in cancer studies whereby a direct correlation has been drawn between starting cell densities and drug efficacy (31). In other works, TAT has documented measurable cytotoxicity above 10 µM (32) and our metabolic assays employed herein showed no to low cytotoxicity from TAT-CaM

316 treatment only. Collectively, these data support that CBS-E2 mediated the observed phenotypes
317 post-delivery.

318 CBS-E2 failed to inhibit cellular proliferation or induce cell death in the human HMEC
319 cell line (**Fig. 5**) supporting previous work showing E2's effects are attributed to interaction with
320 the viral oncoproteins E6 & E7. The mechanism via which E2 mediates these effects, i.e. via direct
321 or indirect interaction with E6 & E7, are still unknown. Desaintes et al. found that senescence and
322 apoptosis could occur within the same cellular population and postulated that these outcomes may
323 be the result of the amount of E2 being made within the cell (16). In this work, the ability to directly
324 deliver protein into cells allowed control over dosage. Our results support a dose-dependent effect
325 model whereby E2 inhibits cellular proliferation at low cell-to-peptide and promotes cell death at
326 high cell-to-peptide ratios. At lower cell-to-peptide ratios we did not readily detect cell death
327 however it is possible this may be a limitation of approach and more sensitive assays would detect
328 both cell death and reduced proliferation within these populations.

329 In summary, this study showed that the TAT-CaM adaptor system effectively delivers
330 CBS-E2 into cultured cells, inhibiting cellular proliferation and inducing cell death. It may hold
331 therapeutic potential as an innovative alternative to transfection or transduction, avoiding problems
332 associated with gene delivery and conferring several advantages including dose control and non-
333 toxicity. This work also lays the foundation for a new approach towards our understanding of the
334 biology of HPV-mediated cervical cancer and studying the specific and interrelated roles of viral
335 proteins in proliferation, senescence and cell death.

336

337 **Author Contributions:** Conceptualization, J.C.L. and J.L.M.; methodology, J.C.L. and J.L.M.; analysis,
338 J.C.L., S.N. and J.L.M.; investigation, J.C.L., H.L.D., R.L.D., L.R.S., J.C.B., S.H. resources, J.L.M..; data curation,
339 J.C.L., J.L.M.; writing—original draft preparation, J.C.L.; writing—review and editing, J.C.L. and J.L.M..;
340 supervision, J.C.L. and J.L.M.; project administration, J.L.M..; funding acquisition, J.C.L. and J.L.M. All
341 authors have read and agreed to the published version of the manuscript.

342 **Funding:** This work was primarily funded by Public Health Service grant R15 EB028609. This
343 work was also supported by Public Health Service grants R16 GM 145448 and R15 HL 161738 to
344 S.J.N. H.L.D. was supported by a Birla Carbon Fellowship from Kennesaw State University

College of Science & Mathematics, Kennesaw, GA. J.C.B. was supported by a Mentor-Protegee grant from Kennesaw State University College of Science & Mathematics, Kennesaw, GA.

References

1. LaVigne AW, Triedman SA, Randall TC, Trimble EL, Viswanathan AN. Cervical cancer in low and middle income countries: Addressing barriers to radiotherapy delivery. Gynecologic oncology reports. 2017;22:16-20.
2. Doorbar J, Quint W, Banks L, Bravo IG, Stoler M, Broker TR, et al. The Biology and Life-Cycle of Human Papillomaviruses. Vaccine. 2012;30:F55-F70.
3. Mantovani F, Banks L. The human papillomavirus E6 protein and its contribution to malignant progression. Oncogene. 2001;20:7874-87.
4. Munger K, Basile JR, Duensing S, Eichten A, Gonzalez SL, Grace M, et al. Biological activities and molecular targets of the human papillomavirus E7 oncoprotein. Oncogene. 2001;20(54):7888-98.
5. Bernard BA, Bailly C, Lenoir MC, Darmon M, Thierry F, Yaniv M. The human papillomavirus type 18 (HPV18) E2 gene product is a repressor of the HPV18 regulatory region in human keratinocytes. J Virol. 1989;63(10):4317-24.
6. Gammoh N, Grm HS, Massimi P, Banks L. Regulation of Human Papillomavirus Type 16 E7 Activity through Direct Protein Interaction with the E2 Transcriptional Activator. Journal of Virology. 2006;80(4):1787.
7. Grm HS, Massimi P, Gammoh N, Banks L. Crosstalk between the human papillomavirus E2 transcriptional activator and the E6 oncoprotein. Oncogene. 2005;24(33):5149-64.
8. Dürst M, Kleinheinz A, Hotz M, Gissmann L. The Physical State of Human Papillomavirus Type 16 DNA in Benign and Malignant Genital Tumours. Journal of General Virology. 1985;66(7):1515-22.
9. Schwarz E, Freese UK, Gissman, L., Mayer W, Roggenbuck B, Stremlau A, zur Hausen H. Structure and transcription of human papillomavirus sequences in cervical carcinoma cells. Nature. 1985;314(6006):111-4.
10. Romanczuk H, Howley PM. Disruption of either the E1 or the E2 regulatory gene of human papillomavirus type 16 increases viral immortalization capacity. Proceedings of the National Academy of Sciences. 1992;89(7):3159.
11. Jeon S, Allen-Hoffmann BL, Lambert PF. Integration of human papillomavirus type 16 into the human genome correlates with a selective growth advantage of cells. J Virol. 1995;69(5):2989-97.
12. Wagatsuma M, Hashimoto K, Matsukara T. Analysis of integrated human papillomavirus type 16 DNA in cervical cancers: amplification of viral sequences together with cellular flanking sequences. J Virol. 1990;64(2):813-21.
13. Hwang ES, Riese DJ, Settleman J, Nilson LA, Honig J, Flynn S, et al. Inhibition of cervical carcinoma cell line proliferation by the introduction of a bovine papillomavirus regulatory gene. Journal of Virology. 1993;67(7):3720.
14. Dowhanick JJ, McBride AA, Howley PM. Suppression of cellular proliferation by the papillomavirus E2 protein. J Virol. 1995;69(12):7791-9.
15. Goodwin EC, Naeger LK, Breiding DE, Androphy EJ, DiMaio D. Transactivation-competent bovine papillomavirus E2 protein is specifically required for efficient repression of human papillomavirus oncogene expression and for acute growth inhibition of cervical carcinoma cell lines. J Virol. 1998;72(5):3925-34.
16. Desaintes C, Demeret C, Goyat S, Yaniv M, Thierry F. Expression of the papillomavirus E2 protein in HeLa cells leads to apoptosis. EMBO J. 1997;16(3):504-14.

17. Webster K, Parish J, Pandya M, Stern PL, Clarke AR, Gaston K. The human papillomavirus (HPV) 16 E2 protein induces apoptosis in the absence of other HPV proteins and via a p53-dependent pathway. J Biol Chem. 2000;275(1):87-94.
18. Das SK, Menezes ME, Bhatia S, Wang X-Y, Emdad L, Sarkar D, et al. Gene Therapies for Cancer: Strategies, Challenges and Successes. Journal of Cellular Physiology. 2015;230(2):259-71.
19. Roeder GE, Parish JL, Stern PL, Gaston K. Herpes simplex virus VP22-human papillomavirus E2 fusion proteins produced in mammalian or bacterial cells enter mammalian cells and induce apoptotic cell death. Biotechnol Appl Biochem. 2004;40(Pt 2):157-65.
20. Green KL, Southgate TD, Mulryan K, Fairbairn LJ, Stern PL, Gaston K. Diffusible VP22-E2 protein kills bystander cells and offers a route for cervical cancer gene therapy. Hum Gene Ther. 2006;17(2):147-57.
21. Lecher JC, Nowak SJ, McMurry JL. Breaking in and busting out: Cell-penetrating peptides and the endosomal escape problem. Biomol Concepts. 2017;8(3-4):131-41.
22. Salerno JC, Ngwa VM, Nowak SJ, Chrestensen CA, Healey AN, McMurry JL. Novel cell penetrating peptides effect intracellular delivery and endosomal escape of desired protein cargos. J Cell Sci. 2016;129(5):893-7.
23. Ngwa VM, Axford DS, Healey AN, Nowak SJ, Chrestensen CA, McMurry JL. A versatile cell-penetrating peptide-adaptor system for efficient delivery of molecular cargos to subcellular destinations. PloS one. 2017;12(5):e0178648.
24. Gentry SB, Nowak SJ, Ni X, Hill SA, Wade LR, Clark WR, et al. A real-time assay for cell-penetrating peptide-mediated delivery of molecular cargos. PLoS One. 2021;16(9):e0254468.
25. Van Tine BA, Dao LD, Wu SY, Sonbuchner TM, Lin BY, Zou N, et al. Human papillomavirus (HPV) origin-binding protein associates with mitotic spindles to enable viral DNA partitioning. Proc Natl Acad Sci USA. 2004;101(12):4030-5.
26. Mahmood T, Yang PC. Western blot: technique, theory, and trouble shooting. N Am J Med Sci. 2012;4(9):429-34.
27. Dao LD, Duffy A, Van Tine BA, Wu S-Y, Chiang C-M, Broker TR, et al. Dynamic Localization of the Human Papillomavirus Type 11 Origin Binding Protein E2 through Mitosis While in Association with the Spindle Apparatus. Journal of Virology. 2006;80(10):4792.
28. Muller M, Jacob Y, Jones L, Weiss A, Brino L, Chantier T, et al. Large Scale Genotype Comparison of Human Papillomavirus E2-Host Interaction Networks Provides New Insights for E2 Molecular Functions. PLOS Pathogens. 2012;8(6):e1002761.
29. McMurry JL, Chrestensen CA, Scott IM, Lee EW, Rahn AM, Johansen AM, et al. Rate, affinity and calcium dependence of CaM binding to eNOS and nNOS: effects of phosphorylation. FEBS J. 2011;278(24):4943-54.
30. Bellanger S, Blachon S, Mechali F, Bonne-Andrea C, Thierry F. High-Risk But Not Low-Risk HPV E2 Proteins Bind to the APC Activators Cdh1 and Cdc20 and Cause Genomic Instability. Cell Cycle. 2005;4(11):1608-15.
31. Lica JJ, Wieczor M, Grabe GJ, Heldt M, Jancz M, Misiak M, et al. Effective Drug Concentration and Selectivity Depends on Fraction of Primitive Cells. Int J Mol Sci. 2021;22(9).
32. Cardozo AK, Buchillier V, Mathieu M, Chen J, Ortis F, Ladriere L, et al. Cell-permeable peptides induce dose- and length-dependent cytotoxic effects. Biochim et Biophys Acta. 2007;1768(9).

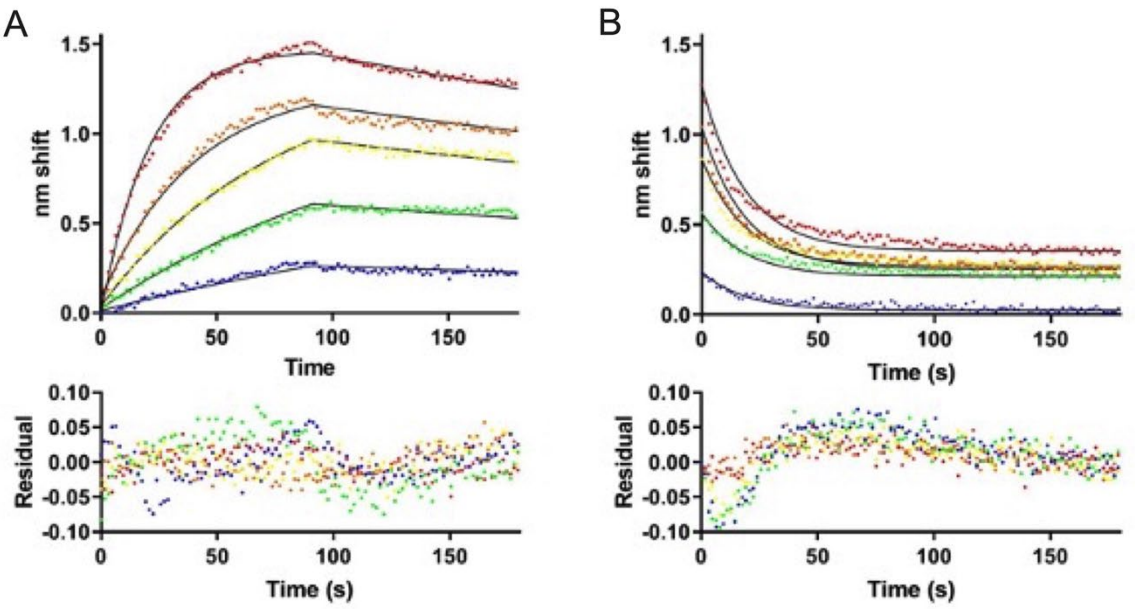

Figure 1. Biolayer interferometry analysis of TAT-CaM binding to CBS-E2. A) Association-then-dissociation experiment in which ligand TAT-CaM was exposed to varying concentrations of CBS-E2 prior to movement to buffer only at 90s (red, 1000 nM; orange, 500 nM; yllow, 250 nM, green, 125 nM, blue 63 nM). Data points are individual instrument readings. Lines represent best fits to a global single-state model. Residuals are shown below. B) The same samples after dissociation were moved to buffer containing 10 mM EDTA for monitoring of dissociation in the absence of Ca^{2+}. Fits are to a global single-state exponential decay model. Residuals indicate some non-ideality in the model, likely due to rapid dissociation prior to the first reading (see discussion).

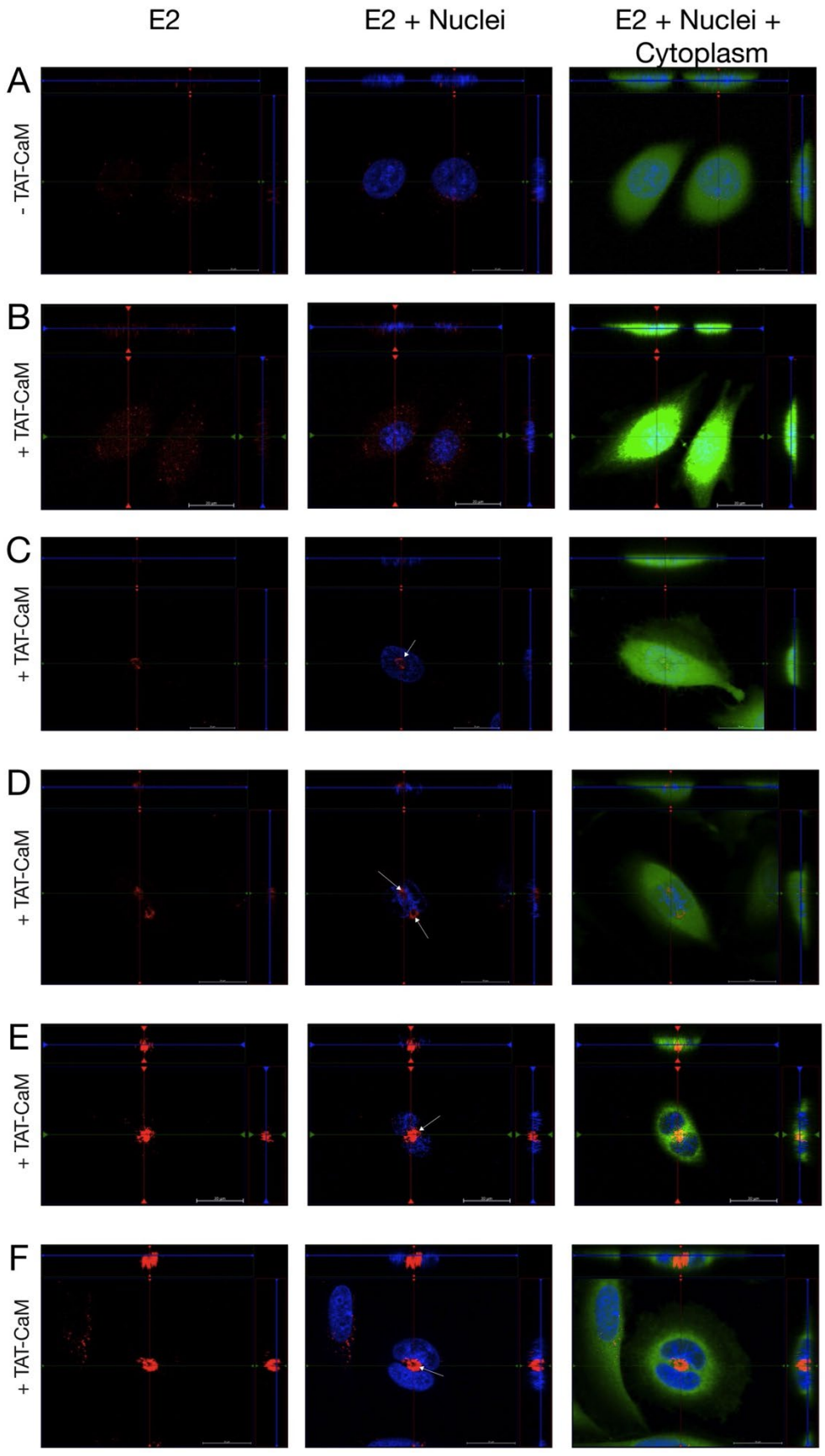
E2
E2 + Nuclei
E2 + Nuclei + Cytoplasm
A
- TAT-CaM
B
+ TAT-CaM
C
+ TAT-CaM
D
+ TAT-CaM
E
+ TAT-CaM
F
+ TAT-CaM

447

Figure 2. Delivery of CBS-E2 into living cervical cancer cells via the TAT-CaM adaptor. Cervical cancer cells were incubated with fluorescently labeled CBS-E2 cargo (Red) in the absence (A) or presence (B-F) of equimolar TAT-CaM for 1 hr. Cells were counterstained with with NucBlue (nuclei; blue) and Cytotracker (cytoplasm; green). Images were generated on an inverted Zeiss LSM700 Confocal Microscope with Z-stack projections. Shown at the top and right of each image are orthogonal projections taken at the depth of the nucleus. A, B) Visualization of E2 in SiHas in asynchronous populations. C-F) Visualization of E2 in mitotically active cells. White arrows indicate redistribution and clustering of E2 to regions of the cell typically associated with the mitotic spindle apparatus.

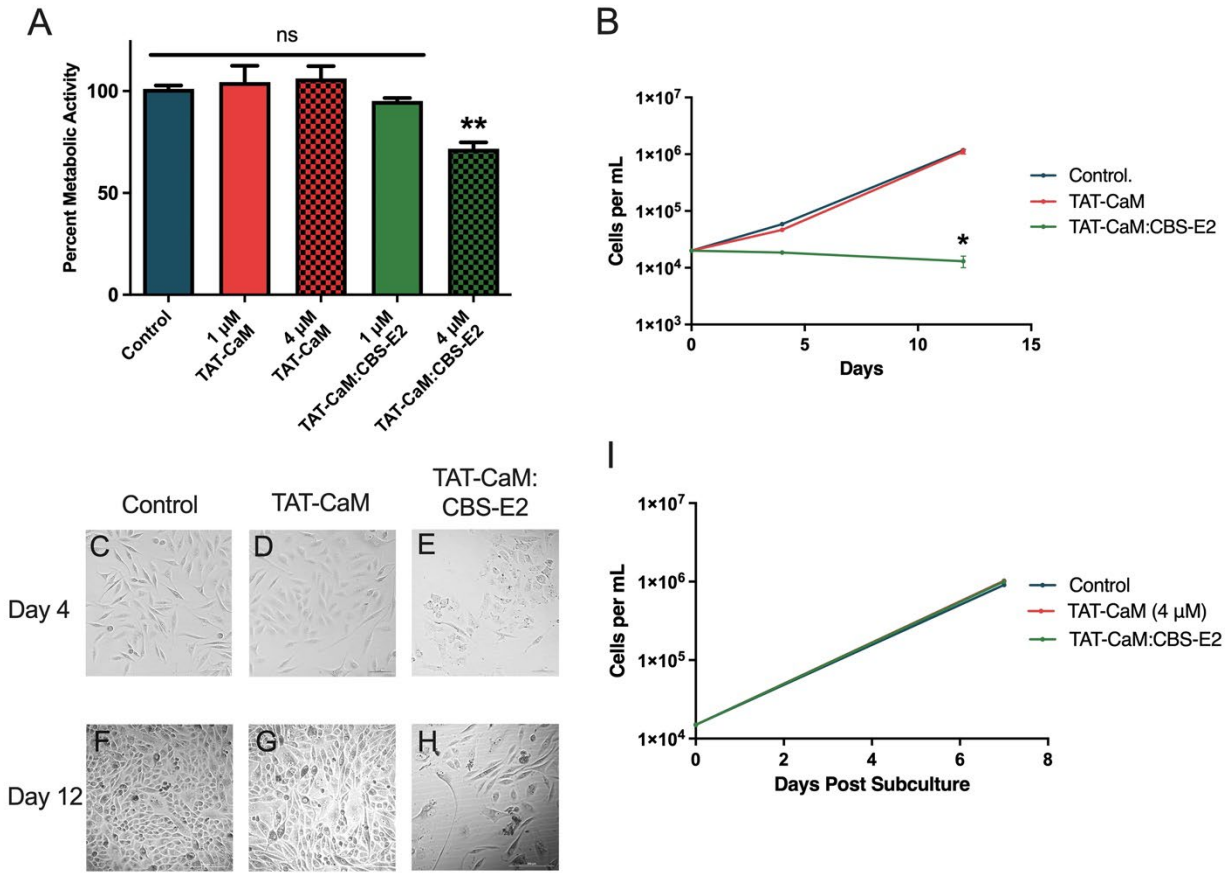

Figure 3. CBS-E2 delivery induces reversible inhibition of cell growth in cervical cancer cells. Cells were seeded at 2.5 x 10^4 per well and treated once daily for three days with either 1 µM or 4 µM CBS-E2 in the presence of equimolar amounts of TAT-CaM. As a control, cells were either left untreated (negative control) or treated with TAT-CaM only (experimental control). A) MTS assay to assess cellular metabolic activity on day 4. A reduction in metabolic activity was tested for by One-way ANOVA with Dunnet's correction for multiple comparisons *p = 0.03. n = 9; shown SEM. B) On day 4 and day 12, cells were collected and counted on a hemocytometer. Data was analyzed by Two-way ANOVA with Dunnet's correction for multiple comparisons *p = 0.02. n=4; shown SEM. C-H) Micrographs of cells from each treatment group on day 4 and day 12 post treatment. Images are from the 4 µM treatments. I) On day 12, cells were collected and reseeded at equal density and cultured for an additional week after which they were collected and counted on a hemocytometer. n = 4.

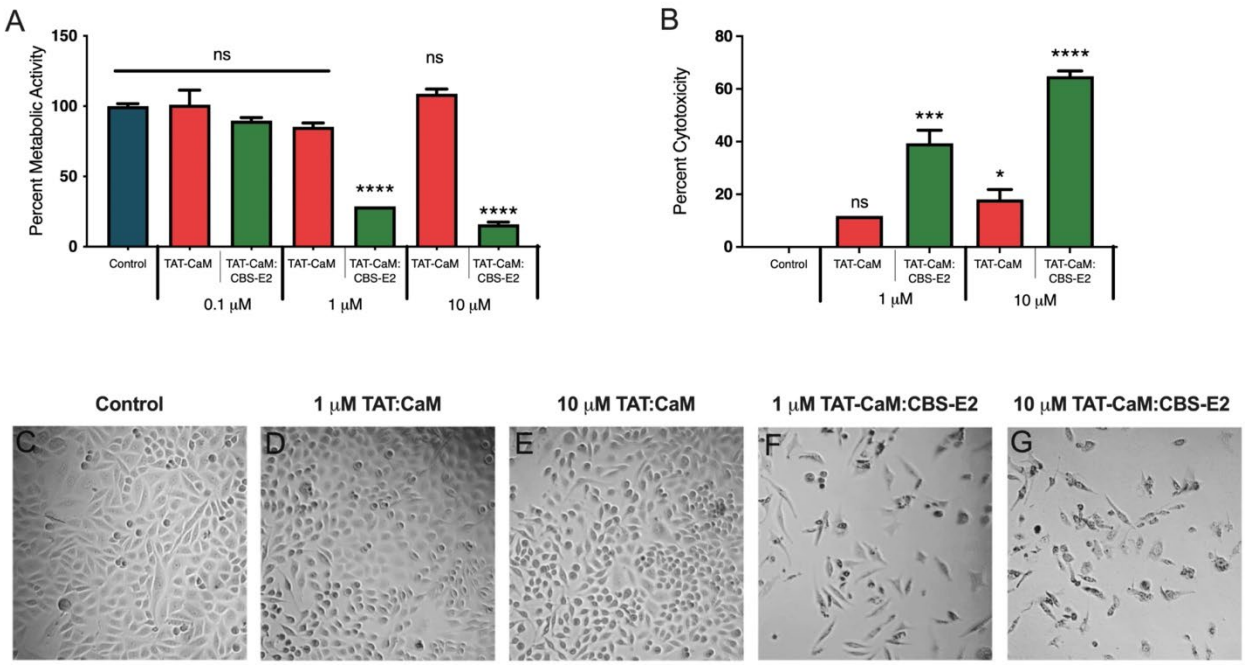

488

489 **Figure 4. CBS-E2 induces cell death in cervical cancer cells**. Cells were seeded at 2.5 x 10^3
490 and treated once daily for three days with either 1, 3 or 10 μM E2 in the presence of equimolar
491 amounts of TAT-CaM. As a control, cells were either left untreated (negative control) or treated
492 with TAT-CaM only (experimental control). A) MTS assay to assess cellular metabolic activity
493 on day 4. A reduction in metabolic activity was tested for by One-way ANOVA with Dunnet's
494 correction for multiple comparisons ****$p < 0.001$. n=9; shown SEM. B) LDH leakage assay to
495 assess cytotoxicity on day 4. Percent cytotoxicity was tested for by One-way ANOVA with
496 Dunnet's correction for multiple comparisons *$p = 0.024$, ***$p = 0.008$, ****$p < 0.001$. n = 9;
497 shown SEM. C-G) Micrographs of cells from each treatment group taken on day 4.
498
499
500
501
502
503
504
505
506

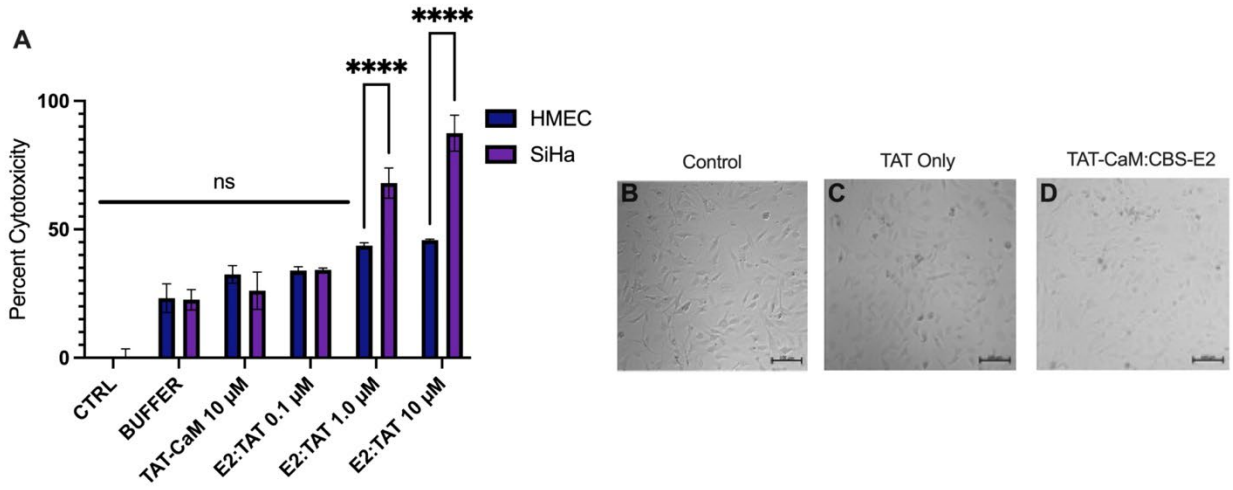

Figure 5. CBS-E2 does not induce cell death in human microvascular endothelial cells. SiHa and HMEC cells were seeded at 2.5 x 10^3 and treated once daily for three days with 10 µM E2 in the presence of equimolar amounts of TAT-CaM. As a control, cells were either left untreated (negative control), treated with NEB buffer (treatment control), or treated with TAT-CaM only (experimental control). A) LDH leakage assay to assess cytotoxicity on day 4. Percent cytotoxicity were tested for by One-way ANOVA with Dunnet's correction for multiple comparisons. n = 4; shown SEM. ****$p < 0.000.1$ B-D) Micrographs of cells from each treatment group taken on day 4.

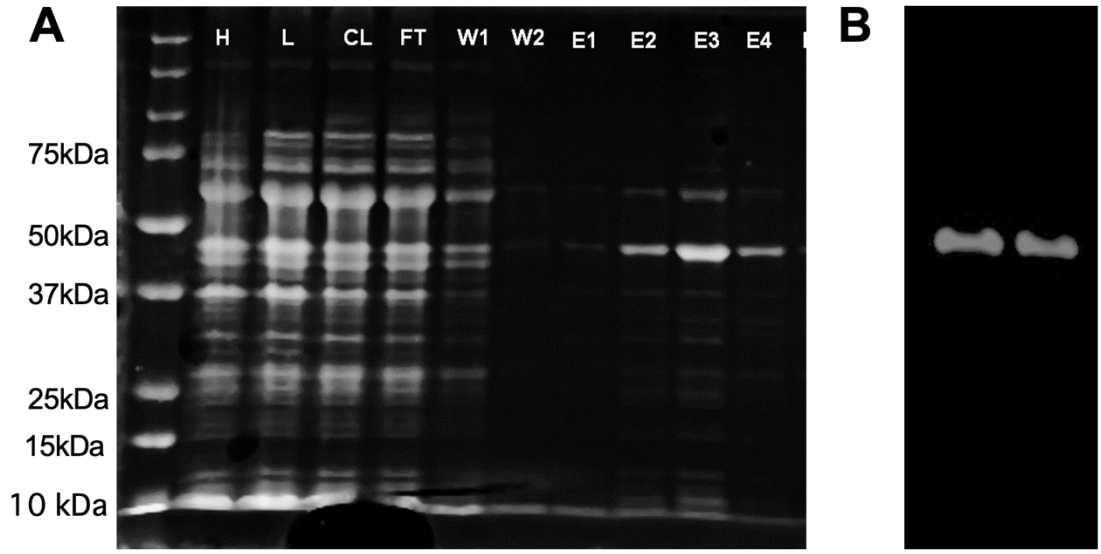

Supplemental Figure 1: Protein purification of CBS-E2. E2 was expressed $i^{1}n^{5kD}E^{a}$.*coli* BDP competent strain with lysis buffers containing 1 mM EDTA and 2 mM $CaCl_2$. A) Gel Electrophoresis. Un = uninduced; In = induced; H – homogenate; L = lysate; Cl = clarified lysate; FT = flow through; W = washes; EL/E = elutions. B) Western blot of elutions 2 & 3 for E2.

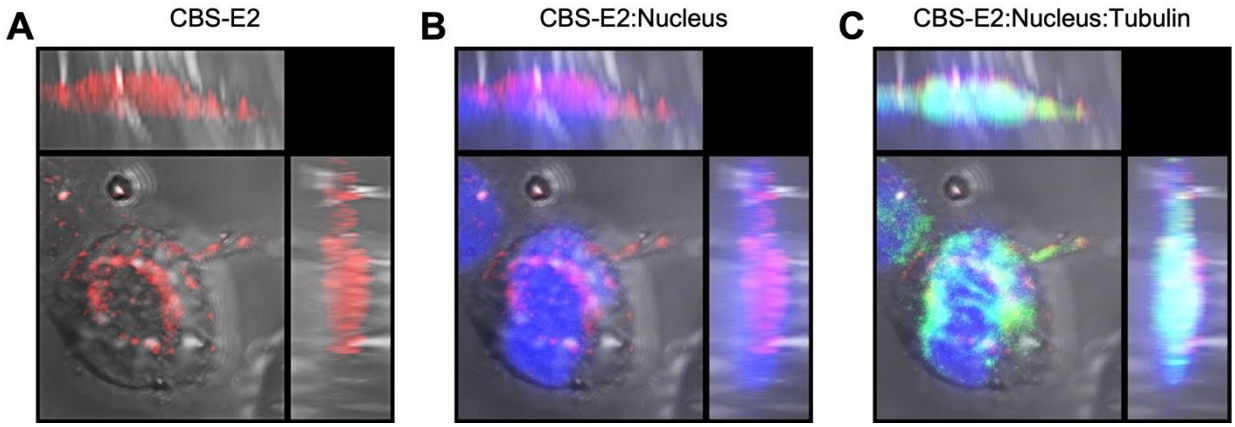

Supplemental Figure 2: Co-Localization of CBS-E2 and Tubulin with the Nucleus in SiHa cells. Cervical cancer cells (SiHa) were incubated with fluorescently labeled CBS-E2 cargo (red) in the presence of equimolar TAT-CaM for 1 hr. Cells were counterstained with NucBlue (nuclei; blue) then fixed with ice-cold 100% methanol for 3 minutes. Post fixation, cells were probed for beta-tubulin (primary) and detected with a secondary GFP-conjugate (green). Images were generated on an inverted Zeiss LSM700 Confocal Microscope with Z-stack projections. Shown at the top and right of each image are orthogonal projections taken at the depth of the nucleus.